Original Article

Uwa O. Uyor*, Patricia A. I. Popoola and Olawale M. Popoola

Network structural hardening of polypropylene matrix using hybrid of OD, 1D and 2D carbon-ceramic nanoparticles with enhanced mechanical and thermomechanical properties

https://doi.org/10.1515/polyeng-2021-0216 Received July 23, 2021; accepted February 15, 2022; published online April 1, 2022

Abstract: Various dimensional structured inorganic nanoparticles have different ways of improving mechanical properties of polymeric materials. However, there are limited studies on hybridization of different nanoparticles with different dimensional structures for optimal enhancement of mechanical properties of polymer matrix. Therefore, this study combined nanoparticles with 0D (barium titanate [BT]), 1D (carbon nanotubes [C]), and 2D (graphene [G] and boron nitride [BN]) to significantly promote the hardness, elastic modulus, tensile strength/ modulus, heat deflection and Vicat softening temperature of polypropylene (PP) nanocomposites. The nanoparticles were surface functionalized to take care of good interfacial interaction with the PP matrix. The nanocomposites were fabricated via melt compounding techniques. Although all the developed nanocomposites showed enhanced mechanical and thermomechanical properties, the ones containing hybrid of carbon and ceramic nanoparticles with different dimensional structures showed superior responses. For instance, optimal hardness, elastic modulus, heat deflection and Vicat softening temperature of about 269.5 MPa, 2.9 GPa, 100.7 °C, and

*Corresponding author: Uwa O. Uyor, Department of Chemical, Metallurgical and Materials Engineering, Tshwane University of Technology, Pretoria, Private Bag X680, Pretoria, South Africa; and Center for Energy and Electrical Power, Tshwane University of Technology, Pretoria, Private Bag X680, Pretoria, South Africa, E-mail: UyorUO@tut.ac.za. https://orcid.org/0000-0003-2200-2309 Patricia A. I. Popoola, Department of Chemical, Metallurgical and Materials Engineering, Tshwane University of Technology, Pretoria, Private Bag X680, Pretoria, South Africa

Olawale M. Popoola, Center for Energy and Electrical Power, Tshwane University of Technology, Pretoria, Private Bag X680, Pretoria, South Africa; and Department of Electrical Engineering, Tshwane University of Technology, Pretoria, Private Bag X680, Pretoria, South Africa

160 °C were measured for the hybrid PP/3 wt%BNG/3 wt%BTC nanocomposite, which are about 239.4%, 77.7%, 19 °C, and 11 °C higher than that of the pure PP, respectively. The significant enhancement in the measured properties is attributed to effective mechanical interlocking and network structural hardening of the PP matrix.

Keywords: hardness; modulus; polypropylene; tensile strength; thermomechanical properties.

1 Introduction

For the past years, there have been tremendous research outputs for the improvement of mechanical properties of polymers using ceramic fillers [1] carbon fillers [2] and organic fillers [3]. Composites' design and development have shown good potential in improving mechanical properties of polymers via controlling and restraining their chains on applications of load. In this nanotechnological era, the use of nanofillers to improve mechanical properties of polymers is a welcome development. Nanofillers significantly enhance mechanical and other properties of polymers at a very lower concentration due to their large surface area compared to microfillers. Carbon-based percolative nanofillers such as graphene and carbon nanotubes have shown promising potentials in the enhancement of mechanical, thermal, and electrical properties of polymer nanocomposites due to their high and excellent engineering properties [4, 5]. They are hexagonal nanomaterials with honeycomb structure and carbon atoms in sp² configuration [6, 7]. The graphene and carbon nanotubes are respectively 2D and 1D structural nanomaterials with high aspect ratio, which enables their significant influence on the various properties of polymers at low content. They have good mechanical properties such as Young Modulus of about 1 TPa and strength of 130 GPa and 50 GPa for graphene and carbon nanotubes respectively [8, 9]. However, some of the major challenges associated with this class of nanofillers are incompatibility and agglomeration in the polymer matrix [10], which have significant contribution in deterioration of mechanical properties of such nanocomposites. On that regard, research attention has shifted towards interfacial engineering of carbon percolative nanofillers since interfacial interaction between constituent(s) of composite materials are complicated, which involves simultaneous responses of mechanical, chemical, and physical factors [11]. Promoting their interfacial relationship with polymer matrix is often achieved via surface functionalization or modification, which attaches functional groups on them with enhanced dispersion and engineering properties [5, 12].

On the other hand, ceramic materials such as boron nitride and barium titanate used in this study also have good mechanical properties like strength of about 83 MPa and 100 MPa and Young Modulus of about 100 GPa and 67 GPa respectively [13, 14]. Notwithstanding, most ceramic nanofillers have lower aspect ratio compared to carbon percolative nanofillers, therefore, required significant amount to enhance properties of polymer matrix. For instance, for nanoindentation, high concentration of ceramic nanofillers is required to obtain appreciable contact between an indenter's tip and nanofillers in a polymer matrix for enhance nanomechanical properties [15]. However, such high concentration can deteriorate tensile strength, elongation, flexibility and induce high weight on the resultant polymer nanocomposites. Determination of mechanical properties using nanoindentation approach is currently taking place of conventional means of doing so. This is due to its advantage of measuring mechanical properties of a material on desired locations on a material's surface, which can be related it is microstructure [1]. It employs localized deformation from the surface of a material to few nanometers underneath in the evaluation of nanomechanical properties [16, 17]. This technique has been found suitable for most materials including polymer and their composites. For instance, Rajeshwari and Dey [1] used nanoindentation to determine hardness and elastic modulus of high-density polyethylene nanocomposites, which improved by 219.3% and 242.4% at 20 vol% nano aluminium nitride loading. Chafidz et al. [18] has also used nanoindentation to obtain increase in hardness and reduced modulus of about 36% and 34% with 3 wt% carbon nanotubes in polypropylene (PP) matrix. While Tserpes et al. [19] adopted both tension and nanoindentation approaches in the investigation of mechanical properties of PP/carbon nanotubes with enhanced responses.

Studies on combination of different dimensional structured nanoparticles for the enhancement of mechanical properties of polymer matrix are rare. 0D, 1D, 2D, and 3D nanoparticles have different degree of improving the mechanical properties of polymer matrix due to their different load bearing capability, orientation in the matrix, impeding and interlocking of polymer chains. Therefore, their hybrid can yield optimal mechanical properties through combination of their various structures in network hardening of the polymer matrix. Final properties of polymer nanocomposites often rely on phases present and interfacial relationship between the nanocomposites' constituent(s) [11]. Where hybrid of different structural nanoparticles can assist one another in promoting dispersion and interfacial relationship in the polymer matrix. Therefore, the aim of this study is to obtain high mechanical and thermomechanical properties at low content without sacrificing tensile properties of PP nanocomposites, by using hybrid OD (barium titanate), 1D (carbon nanotubes), and 2D (graphene and boron nitride). In that regard, this study experimentally showed that the hybridization aided in good dispersion of the nanoparticles in the PP matrix and enhanced its tensile, nanomechanical and thermomechanical properties more than the nanocomposites containing only graphene and carbon nanotubes. This was due to the combined effect of the carbon and ceramic nanoparticles in network structural hardening and stiffening of the PP matrix, respectively.

2 Materials and methods

2.1 Materials

Polypropylene (PP) (melt index - 4 g/10 min, 230 °C/2.16 kg, density -900 kg/m³), polypropylene grafted maleic anhydride (PPMA) (0.5%, density – 920 kg/m³), dopamine hydrochloride (DA-HCl) (essay >98%, MW - 189.64, BP - 248-250 °C), 3-glycidoxypropyltrimethoxysilane (GPTMS) (BP - 120 °C/2 mmHg), graphene (G) (C - >95%, O - <3%, diameter – 2–3 µm, few nano thickness – 6–8 nm), barium titanate (BT) (assay >99%, particles size <100 nm, density 6080 kg/m³ at 25 °C), and xylene plus ethylbenzene basis (ACS reagent, essay >98.5%) were all purchased from Sigma-Aldrich, South Africa. Other materials such as multi walled carbon nanotubes (C) (purity - >98%, diameter -10-30 nm, length - 5-20 μm) and hexagonal boron nitride (BN) (assay >99.5%, particles size <100 nm and density 2200 kg/m³ at 25 °C) were acquired from Hongwu International Group, China.

2.2 Nanoparticle surface modification

The carbon and ceramic nanoparticles used for this study were surface modified using DA-HCl and GPTMS, respectively. 5 g of graphene (G) and carbon nanotubes (C) each were dispersed in two beakers with distilled water and ultrasonicate for 4 h at 80 °C. 2.5 mL of ammonia solution was added into the mixture in dropwise and

further ultrasonicate for 10 h at the same temperature. The mixtures underwent self-polymerization of DA-HCl into polydopamine (PDA) in the presence of the carbon nanoparticles snice the PH of the solution was increase by introducing the ammonia solution. At the end of 10 h, the carbon nanoparticles were severally washed with distilled water to remove unreacted DA-HCl and obtained functionalized graphene (fG) and functionalized carbon nanotubes (fC). Similar process was followed in the functionalization of boron nitride (BN) and barium titanate (BT). Typically, 20 g of BN and BT each were dispersed in separate beakers containing xylene and ultrasonicate for 4 h at 80 °C. Then 50 mL of GPTMS was introduced into each mixture and further ultrasonicated for 10 h. At the end of the reaction, the ceramic nanoparticles were collected and washed severally in a distilled water to remove unreacted GPTMS. Then functionalized BN (fBN) and functionalized BT (fBN) were obtained and tried in an oven. To ensure good interface interaction between the carbon and ceramic nanoparticles, they were combined in groups via hydrothermal and nanoparticles self-assembly methods. The 2D BN and G were mixed in the ratio of 3 wt%G to 15 wt%BN in distilled water and ultrasonicated for 4 h at 80 °C. The mixture was further sealed with aluminium foil and placed in an oven for 10 h at 140 °C for self-assembly of the BN and G (BNG). Also, BT and C were mixed in the ratio of 3 wt%C to 15 wt%BT and followed similar process described above for BNG to obtain self-assembled BT and C (BTC).

2.3 Nanocomposite preparation

The nanocomposites preparation followed easy steps involving masterbatch preparation via solution mixing and melt compounding with pure PP. Typically, for each nanocomposite, certain amount of nanoparticles (denoted as xBNG, xBTC, xG, and xC, where x is the weight percent [wt%]) was mixed with PPMA compatibilizer, which was dissolved in xylene at 130 °C in preparation of PPMA/ nanoparticles masterbatch. The use of PPMA is to enhance compatibility of the nanoparticles with the PP matrix. The PPMA/nanoparticles were mixed for 1 h, dried in an oven and granulated for nanocomposites fabrication. The nanocomposites were developed via melting mixing of the prepared masterbatch and pure PP using HAAK rheomixer 600 OS. Both the masterbatch and appropriate amount of the pure PP were simultaneously fed into the rheomixer and mixed for 10 min at 190 °C and 100 rpm. To obtain consolidated nanocomposites' shapes required for the various analyses conducted in this study, the melt compounded nanocomposites were grinded and hot-pressed using carver presser for 10 min at 200 °C and 10 MPa.

2.4 Characterization procedures

Thermogravimetry analysis (TGA) of the nanoparticles was conducted using TA instrument Q500 to determine if they were successfully functionalized. The analysis was conducted in an inert environment (nitrogen) at a heating rate of 10 °C/min from 50 °C to 900 °C. Fourier Transform Inferred (FTIR) (Perkin Elmer Precise Spectrum 100) was used for the investigation of the functionalized and unfunctionalized nanoparticles. Attenuated total reflection mode was used at wavenumber range of 400–2000 cm⁻¹. Dimensional structures (0D, 1D, and 2D) of the nanoparticles were revealed using transmission electron microscope (TEM) (IEM-2100). The TEM analysis was conducted at acceleration voltage of 200 kV and beam current of 110 μ A.

Microstructures and the state of nanoparticles dispersion in the PP matrix were revealed using scanning electron microscope (SEM) (VEGA 3 TESCAN) at acceleration voltage of 20 kV. Differential scanning calorimeter (DSC) (DSC-Q2000) was used for the investigation of the DSC properties of the nanocomposites in a nitrogen atmosphere at a heat and cooling rate of 10 °C/min. Percentage crystallinity (X_c) was calculated using Eq. (1). Where $\triangle H_f$ is the melting enthalpy of a 100% crystalline form of PP (209 J/g) [20] and $\triangle H_{\rm m}$ is the heat of fusion (J/g).

$$X_c = \frac{\triangle H_{\mathbf{m}}}{\triangle H_f * \mathbf{w} t \%} *100 \tag{1}$$

Tensile properties of the nanocomposites were determined using universal testing machine (LLOYD EZ50) at a crosshead of 5 mm/min for all the samples. The measurement was repeated five times per sample in accordance with ASTM D638 (Type V) standard. The heat deflection temperature (HDT) and Vicat softening temperature (VST) of the nanocomposites were measured in accordance with ASTM D648 standard using HDT/Vicat tester (CEAST HV6). This was done by applying load of 0.45 MPa and heating rate of 2 °C/min, starting from 30 °C to deflection or softening temperature of the samples. The HDT was measured when the nanocomposites deflected by 0.25 mm. The VST was measured in accordance with ASTM D1525 standard at applied load of 10 N. The VST was recorded when flat-ended needle of 1 mm² circular cross section penetrated the samples by 1 mm. Each sample was tested three times and their average are presented in this study. Nanoindentation approach was employed in the determination of the nanomechanical properties of the nanocomposites using nanoindenter (Anton Paar, NHT) in accordance with ASTM D785 standard. This was done by applying load of 200 mN, 20 s penetrating, holding, and retracting time each. Each sample was tested five to ten times and their averages are presented. Hardness H (MPa) and elastic modulus EM (MPa) of the nanocomposites were measured following Oliver and Pharr method, which are calculated using Eqs. (2)–(4) [16].

$$H = \frac{F}{A} \tag{2}$$

$$H = \frac{F}{A}$$

$$EM = \frac{1 - \mathcal{V}^2}{\frac{1}{E_r} - \frac{1 - \mathcal{V}^2}{E_l}}$$

$$E_r = \frac{S\sqrt{\pi}}{2\beta\sqrt{A}}$$

$$(2)$$

$$(3)$$

$$E_r = \frac{S\sqrt{\pi}}{2B\sqrt{A}} \tag{4}$$

where F is the maximum applied load (N), A is the contact area which the nanoindenter's tip makes with the material (m^2) , E_i is the nanoindenter's tip elastic modulus (1140 GPa), v_I is the nanoindenter's tip Poisson ratio (0.07), ν is the Poisson ratio of the PP (0.43), E_r is the reduced elastic modulus of the indentation at contact (MPa), and β is a constant based on indenter's tip geometry [21].

3 Results and discussion

3.1 TGA analysis

Both the carbon and ceramic nanoparticles revealed successful functionalization as presented by their TGA analysis in Figure 1(a). All the functionalized nanoparticles showed different thermal response compared to their pristine states. The carbon nanotubes (C) and graphene

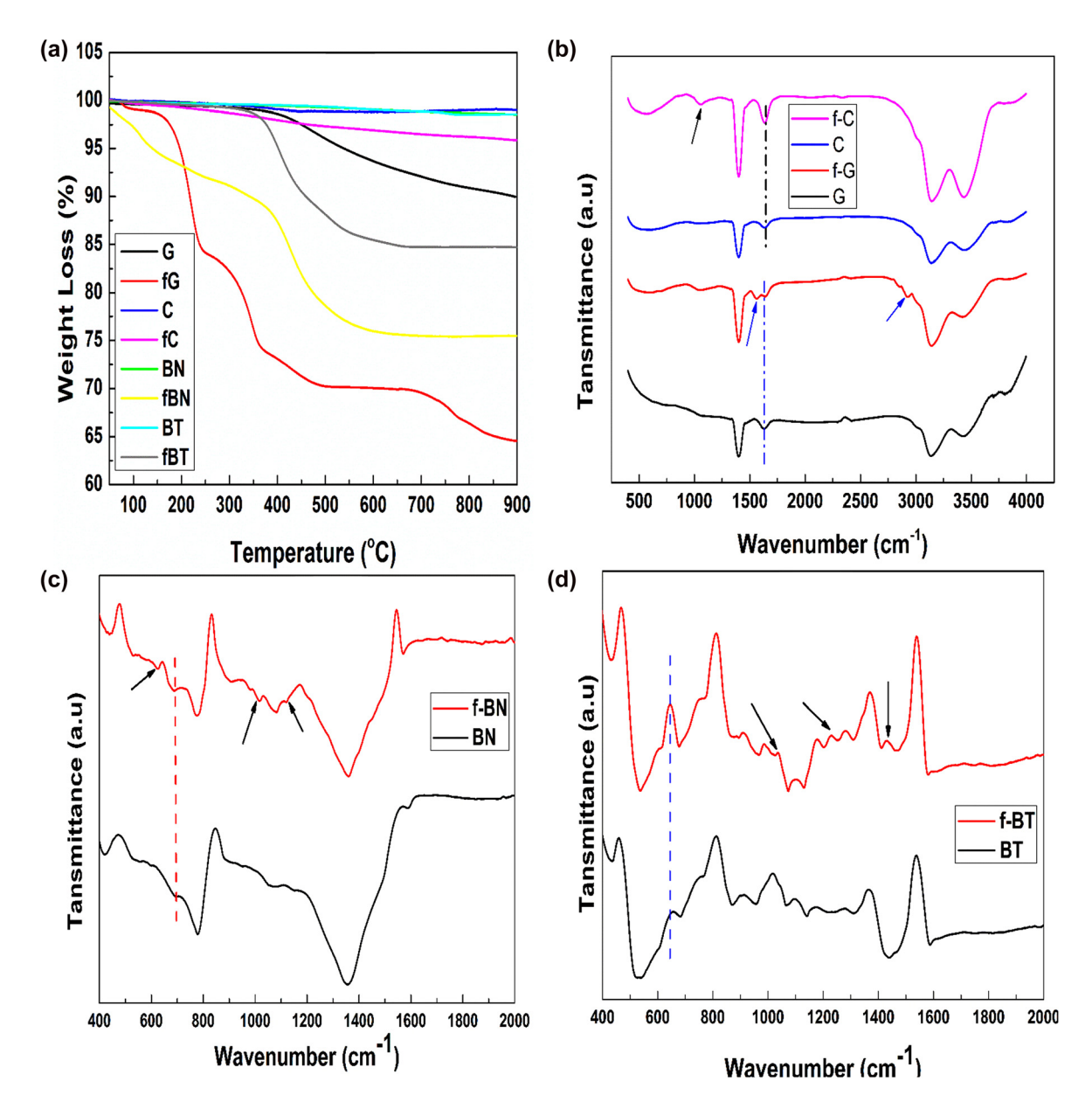


Figure 1: Thermal analysis: (a) TGA analysis of the nanoparticles; FTIR analysis of: (b) G, fG, C, fC, (c) BN, fBN and (d) BT, fBT nanoparticles.

(G) have high thermal stability, which reduced after modification with organic materials due to thermal decomposition of the attached organic matters [22, 23]. The G showed lower decomposition as the temperature increases compared to the C. This is because the G was slightly oxidized on purchase, therefore, thermal decomposition of oxygen and water content resulted to its lower thermal stability. At 900 °C, the C showed only about 1 wt% loss, while the G had about 10 wt% loss as depicted in Figure 1(a). However, after the functionalization process, the wt% loss increased to about 5 wt% and 35.5 wt% at 900 °C for the fC and fG respectively. The increase in the wt% loss of the nanoparticles indicates decomposition of

residual solvent, PDA grafted on the nanoparticles and other organic functional groups [24, 25]. The fG showed more stages of thermal decomposition and higher wt% loss compared to fC. This tells that the fG was more functionalized than fC since it was slight oxidized which increase its affinity with the DA-HCl used for the functionalization. From the TGA analysis, it can be estimated that about 25.5 wt% and 4 wt% organic functional groups were grafted onto the fG and fC, respectively, which indicate their successful functionalization. In the similar way, the TGA analysis of the BN and BT nanoparticles showed that they were also successfully functionalized as include in Figure 1(a). Most ceramic materials including BN and BT

are high thermal stability materials, which show only slight reduction in weight at high temperature [26, 27]. Therefore, at 900 °C, the BN and BT had only about 1.3 wt% and 1.6 wt% loss, respectively. However, fBN and fBT showed different thermal decomposition stages and lower thermal stability compared to their pristine states. This is also as results of quick thermal disintegration of oxygen and other functional groups such as silicon from the GPTMS used for their functionalization. At 900 °C, the fBN and fBT loss about 25 wt% and 15.3 wt% respectively. Therefore, from their TGA analysis, it can be calculated that about 23.7 wt% and 13.7 wt% functionalities from GPTMS were grafted onto the fBN and fBT, respectively, which also indicates successful surface functionalization. This was further confirmed using FTIR analysis as presented in Figure 1(b)–(d). The G and C showed typical graphitic peak vibrations at approximately 1401.6 cm⁻¹, 1616.9 cm⁻¹, 3135.85 cm⁻¹, and 3427.3 cm⁻¹ [28]. However, after the surface modification, new vibration bands were noted for fG and fC as indicated with arrows in Figure 1(b). The vibration band at 1048.50 cm⁻¹ and 1555.2 0 cm⁻¹ for fG represent C-O functional group and N-H shearing respectively [25, 29]. While the small peak at 2920.60 cm⁻¹ corresponds to C-H functional group. The fG showed one new vibration peak at about 1048.50 cm⁻¹, which

represents C-O functional group. And the typical graphitic peak intensity became higher for the fC compared to the C. In addition to the typical hexagonal vibration bands for BN, which represent B-N in-plane and B-N-B out-of-plane bending vibrations [30, 31], new vibration bands were seen for fBN at 630.90 cm⁻¹ and 1009.40 cm⁻¹ as indicated with arrows in Figure 1(c), which could be respectively attributed to B-N-O and B-O-H [32]. While the vibration bands at 1119.7 cm⁻¹ and 1061.3 cm⁻¹ could be attributed to saline functional group in GPTMS that was grafted onto fBN [33]. In the same way, fBT revealed successful surface functionalization as new vibration bands (as indicated with arrows in Figure 1(d)) were noted when compared with the pristine BT. Vibration bands at 1035.50 cm⁻¹ and 1100.20 cm⁻¹ for fBT could be attributed to the saline functional groups in GPTMS [33, 34]. While the bending vibration 1170.90 cm⁻¹ to 1429 cm⁻¹ could represent H-O-H group due to water absorption during the surface modification process [34, 35].

3.2 Microstructural analysis

The TEM micrograph in Figure 2(a) shows high aspect ratio and 1D structure of carbon nanotubes. Its also shows long

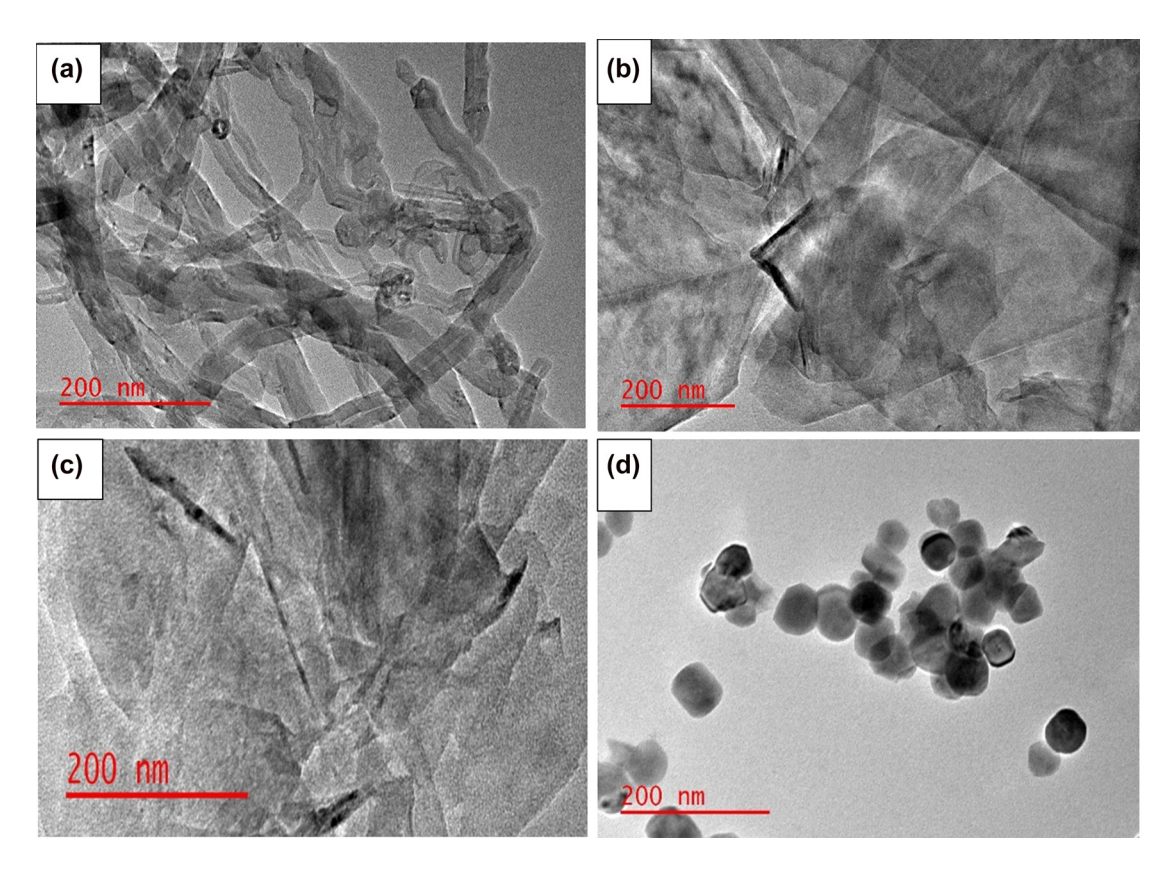


Figure 2: TEM micrographs of (a) the carbon nanotubes, (b) graphene, (c) boron nitride, and (d) barium titanate nanoparticles.

in-plane dimension of nanotubes entangled with one another, which is its typical characteristic [23]. The feature enables formation of network structures in a polymer matrix, which aids in improving mechanical and thermal properties. Large surface of graphene is clearly revealed by the TEM micrograph in Figure 2(b). The figure shows 2D structure with wrinkled surface and large in-plane dimension. Its large in-plane dimension also aids in large surface area for enhancement of mechanical properties of polymer nanocomposites. On the other hand, the BN and BT nanoparticles were also investigated under TEM to ascertain their morphological structures as respectively presented in Figure 2(c) and (d). The BN also has 2D

structure [32] with stacked layers. While TEM micrograph of the BT reveals that BT has OD or spherical structure as depicted in Figure 2(d) [34]. Therefore, the TEM analysis confirms that OD, 1D, and 2D nanostructured materials were used for this study.

The morphological structures of the nanocomposites are presented in Figure 3. The micrographs showed well distribution of the nanoparticles in the PP matrix. This was due to the surface functionalization of the nanoparticles and the use of PPMA compatibilizer in the nanocomposites' preparation. In addition, the use of various nanoparticles with different dimensional structures helped one another in the dispersion. For instance,

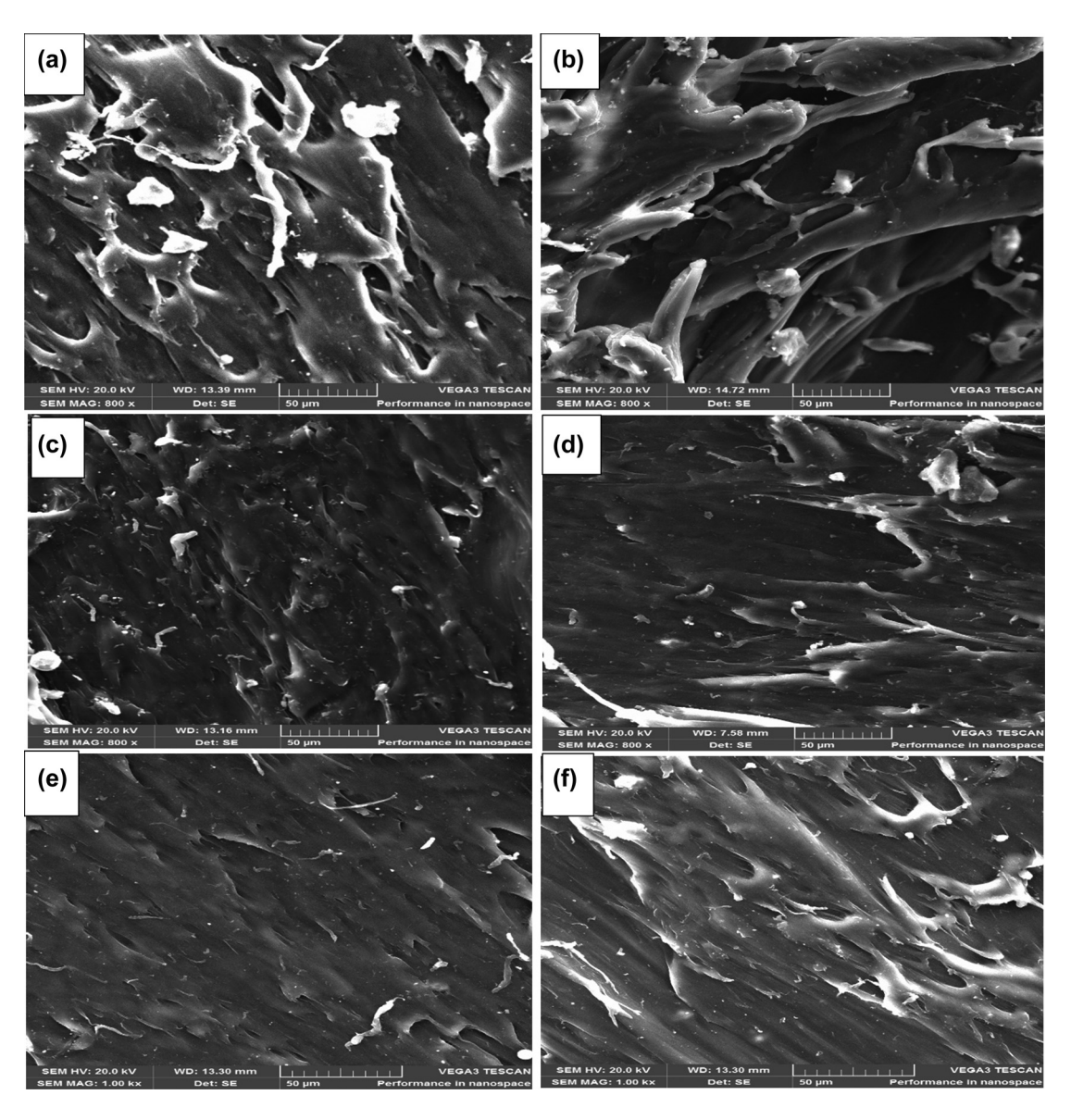


Figure 3: SEM micrographs of nanocomposites containing (a) 1 wt%G/3 wt%C, (b) 3 wt%G/1 wt%C, (c) 1 wt%BNG/1 wt%BTC, (d) 1 wt%BNG/ 3 wt%BTC, (e) 3 wt%BNG/1 wt%BTC, and (f) 3 wt%BNG/3 wt%BTC.

the interpenetration of the G and C reduced the stacking of the G and wall-to-wall interactions of the C in the PP matrix. In the same way, the presence of the BN reduced the stacking of the G sheets, while BT reduced the wall-towall interactions of the C. Hence, relatively good distribution of the nanoparticles in the PP matrix was achieved. The microstructure of PP/1 wt%G/3 wt%C nanocomposite (Figure 3(a)) shows more of mesh-like structure due to the higher content of the 1D structured C. While that of PP/3 wt%G/1 wt%C (Figure 3(b)) shows more of layered structure due to higher content of the 2D structured G. The nanocomposites revealed network-like structures, which resulted to the network structural hardening of the PP matrix with enhanced mechanical properties. However, a better microstructure with no significant separation of the nanoparticles from the matrix was observed for PP/BNG/BTC group as shown in Figure 3(c)–(f). This is an indication that the presence of BN and BT further assisted the dispersion of the G and C in the PP matrix. The microstructures of PP/BNG/BTC nanocomposites group also revealed network-like structures due to the presence of 2D structured G and 1D structured C. In addition, the nanocomposites showed dense morphologies, which can be attributed to the OD structured BT and 2D structured BN nanoparticles since they have relatively higher density compared to the carbon-based nanomaterials. The good dispersion of the nanoparticles in PP/BNG/BTC nanocomposites can be mostly contributed by the presence of the BT nanoparticles since it has smaller size, spherical and 0D structure, which enable it to fill micro-voids in the nanocomposites. Hence, the microstructure of the PP/BNG/BTC group became denser compared to PP/G/C group. Therefore, while the carbon-based nanoparticles gave network structural hardening to the nanocomposites, the ceramic-based nanoparticles further stiffening the PP matrix. This resulted to higher mechanical and thermomechanical properties of the PP/BNG/BTC group compared to the PP/G/C group as recorded in this study.

3.3 DSC properties

The melting temperature (T_m) and crystallization temperature (T_c) of the nanocomposites are shown Figure 4. It can be observed from Figure 4(a) the that the melting peaks of the nanocomposites shifted to the higher temperature relative to the pure PP, which indicates increase in $T_{\rm m}$. The $T_{\rm m}$ increased from 164.3 °C for the pure PP to the range of 167.5 °C-168.9 °C depending on the nanocomposites as presented in the figure. This shows optimal increase of about 4.6 °C for PP-3BN@GNs-3BT@CNTs nanocomposite compared to the pure PP. The recorded $T_{\rm m}$ in this study is higher when compared with those previously reported by other studies [36, 37]. This study credits the enhanced $T_{\rm m}$ to the good relationship between the ceramic nanoparticles (BN/BT) and the carbon nanoparticles (GNs/CNTs) in improving thermal properties of polymer [38] and appreciable distribution of the nanoparticles and their interactions with the matrix as revealed by the SEM micrographs shown in Figure 3. On the other hand, as presented in Figure 4(b), the T_c of the nanocomposites showed more pronounced enhancement when compared with the increase in their $T_{\rm m}$ with respect to the pure PP. Typically, the $T_{\rm c}$ increased from 117.8 °C for the pure PP to optimal of 129.2 °C for PP/1 wt%BNG/3 wt%BTC nanocomposite, which is about 11.4 °C increment. This simply implies that solidification started at higher temperature for the nanocomposites relative to the pure PP. This is due to heterogeneous nucleation in the nanocomposites, where the nanoparticles served as many nucleation sites in the matrix [39, 40]. Other nanocomposites also have higher T_c compared to the pure PP as included in Figure 4(b). The increase in the T_c with respect to the pure PP is very essential in the undercooling reduction and decrease in the crystallization driving force. It is known that when the range between $T_{\rm m}$ and $T_{\rm c}$ is small for polymer composite materials, there may be close distribution of crystallite size within such composites [37]. This probably can be as a result of formation of numerous nucleation sites in the matrix, which serve as barriers in preventing long chains' growth in such nanocomposites. However, formation of many nucleation sites in the matrix with reduction in the crystallite size due to the presence of the nanoparticles promotes the net or effective degree of crystallinity (X_c) of the resultant nanocomposites. Therefore, various studies have attributed increase in X_c of polymer nanocomposites as nucleation effect of the nanoparticles in the polymer matrix [41, 42]. The enhanced X_c of nanocomposites containing PPMA has also been reported just like this study [37, 43]. Hence, X_c increased from 30.4% for the pure PP to optimal of 36.2% for PP/3 wt% BNG/3 wt%BTC nanocomposite. The nanocomposites containing all the three different dimensional structured nanoparticles revealed better X_c , which contributed to their better mechanical and thermomechanical properties compared to PP/G/C nanocomposites.

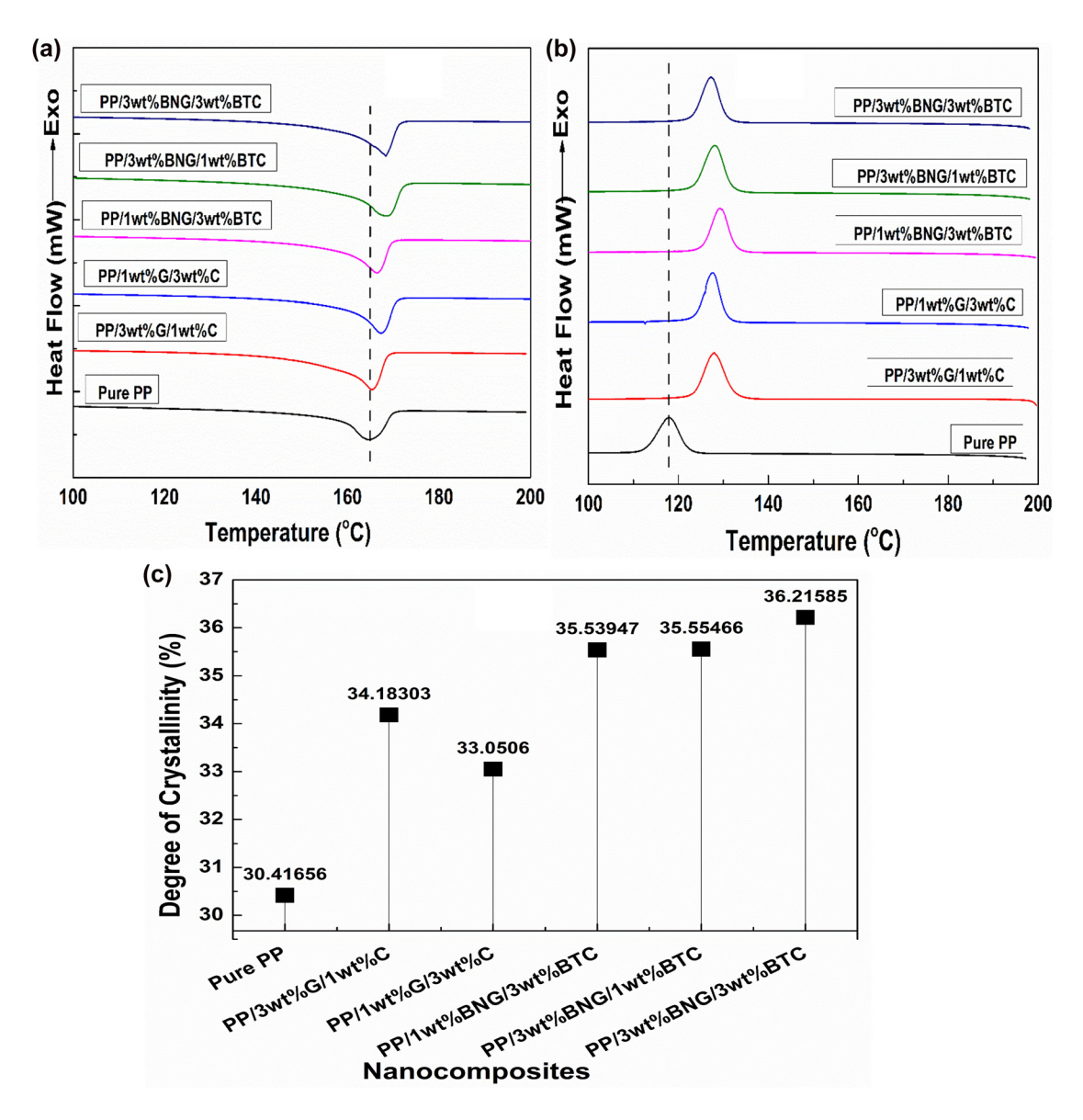


Figure 4: DSC analysis: (a) Melting temperature, (b) crystallization temperature, and (c) degree of crystallinity of the nanocomposites.

3.4 Tensile strength and modulus

Figure 5(a) shows that the tensile strength (TS) of the nanocomposites was improved relative to the pure PP. For instance, TS of about 33.6 MPa was recorded for the pure PP, which increased to about 39.1 MPa for PP/3 wt%BNG/ 3 wt%BTC nanocomposite. This is a significant improvement considering the often reduction in TS of polymer nanocomposites reinforced with percolative carbon nanoparticles, especially at high wt% content due to high level of particles-particles interactions than particles-matrix interactions [44]. Such interactions in combination with formation of nanoparticles aggregates forms localized stress concentration sites and reduction in mechanical

properties of the nanocomposites [45, 46]. PP/1 wt%BNG/ 1 wt%BTC nanocomposite also have higher TS compared to the pure PP and nanocomposites containing only G and C. However, the percentage elongation (PE) of the nanocomposites showed downward characteristic when matched with the pure PP as included in Figure 5(a). This is due to the decrease in ductility or stretchability of the PP chains caused by the nanoparticles' barriers in the matrix. Hence, the flow of PP chains to reasonable extension was restricted. Typically, the PP decreased from 52.7% for the pure PP to the range of 23.0%-20.0% depending on the nanocomposites as depicted in Figure 5(a). It was further noted that reduction in the PE of the PP matrix by addition of the nanoparticles increased its tensile modulus (TM) as

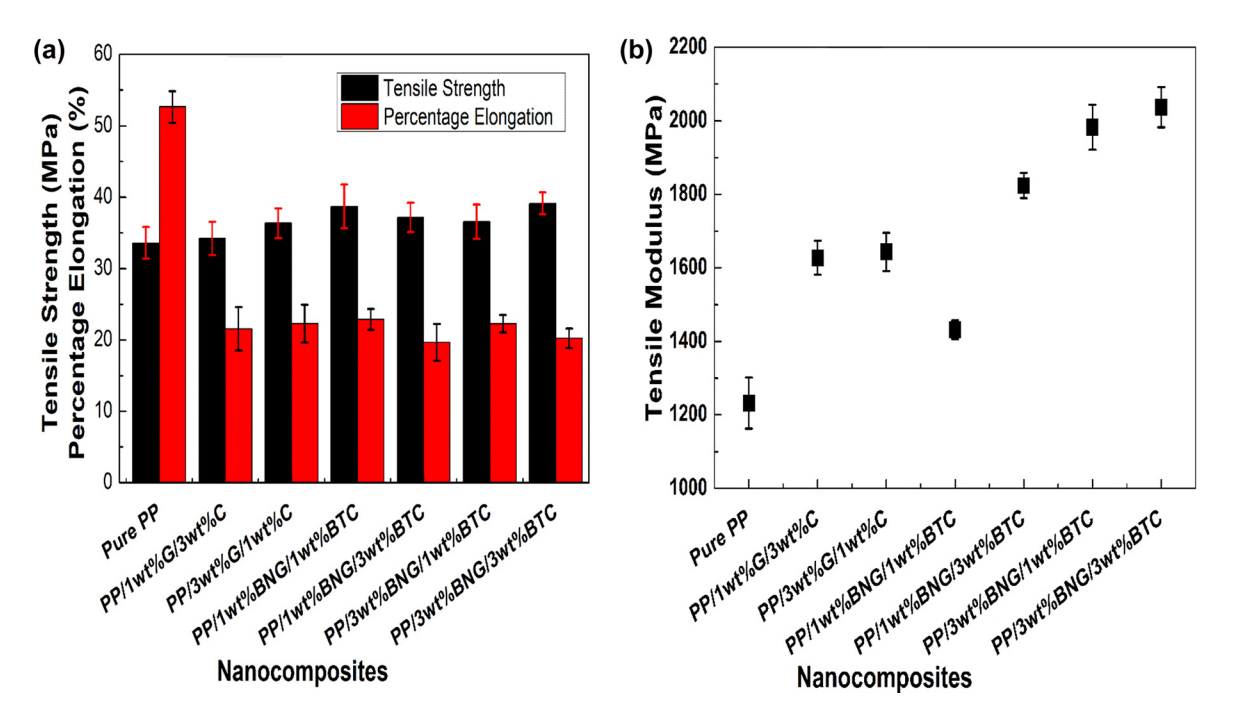


Figure 5: Tensile properties: (a) Tensile strength and (b) tensile modulus of the nanocomposites.

displayed in Figure 5(b). The PP/3 wt%BNG/3 wt%BTC nanocomposite showed optimal TM of about 2037.2 MPa. While about 1231.8 MPa was measured for the pure PP, which amounts to about 65.4% increase. Comparing PP/G/ C group and PP/BNG/BTC group, the latter group showed higher TM than the former group at all similar nanoparticles' concentrations. For instance, TM of about 1627.1 MPa and 1643.6 MPa were, respectively, recorded for the nanocomposites containing 1 wt%G/3 wt%C and 3 wt%G/ 1 wt%C. Which was increased to 1824.1 MPa and 1982.6 MPa for PP/1 wt%BNG/3 wt%BTC and PP/3 wt% BNG/1 wt%BTC, respectively. The enhanced tensile properties were contributed by the good load bearing capability of the hybrid nanoparticles, effective load transfer from the PP matrix to the nanoparticles [44] and good synergetic effect among the nanoparticles with different dimensional structures [47]. The larger TM of the PP/BNG/BTC group compared to the pure PP and PP/G/C nanocomposites implies that they have higher stiffness and resistance to elastic deformation due to effective network structural hardening and mechanical interlocking of the PP chains by BNG and BTC.

3.5 Hardness and elastic modulus

The hardness (H) and elastic modulus (EM) measured for the nanocomposites are represented in Figure 6. The nanocomposites have larger H and EM values compared to

the pure PP. This is in line with their higher TM, confirming the increase in the stiffness of the nanocomposites due to the retrained PP chains and resistance to elastic deformation relative to the pure PP. The enhanced resistance to the elastic deformation was due to the network structural hardening of the PP matrix via retardation of its chains' flow by 3D network structures formation in the matrix by the nanoparticles [48, 49]. The network structural hardening of the PP matrix with enhanced nanomechanical properties were possible due to the good interfacial bonding and dispersion of the nanoparticles in the matrix [50]. From Figure 6, optimal H and EM of about 269.5 MPa and 2.9 GPa were measured for PP/3 wt%BNG/3 wt%BTC nanocomposite, respectively. While about 79.4 MPa and 1.66 GPa were recorded for the pure PP accordingly. These can be quantified to about 239.4% and 77.7% increase in the H and EM for the nanocomposite compared to that of the pure PP. Although PP/G/C group of nanocomposites showed lower H and EM compared to PP/BNG/BTC group at all concentrations, they were still higher than that of the pure PP. The nanocomposites containing 1 wt%BNG/3 wt% BTC and 3 wt%BNG/1 wt%BTC revealed increase in H of about 33.6% and 41.6% and EM of about 29.7% and 25.6% compared to PP/1 wt%G/3 wt%C and PP/3 wt%G/1 wt%C, respectively. These agree with the higher TM for the PP/ BNG/BTC nanocomposites compared to the pure PP and PP/G/C nanocomposites as earlier discussed. This suggests that optimal and more effective network hardening, resistance to deformation and reduction in PP chains mobility

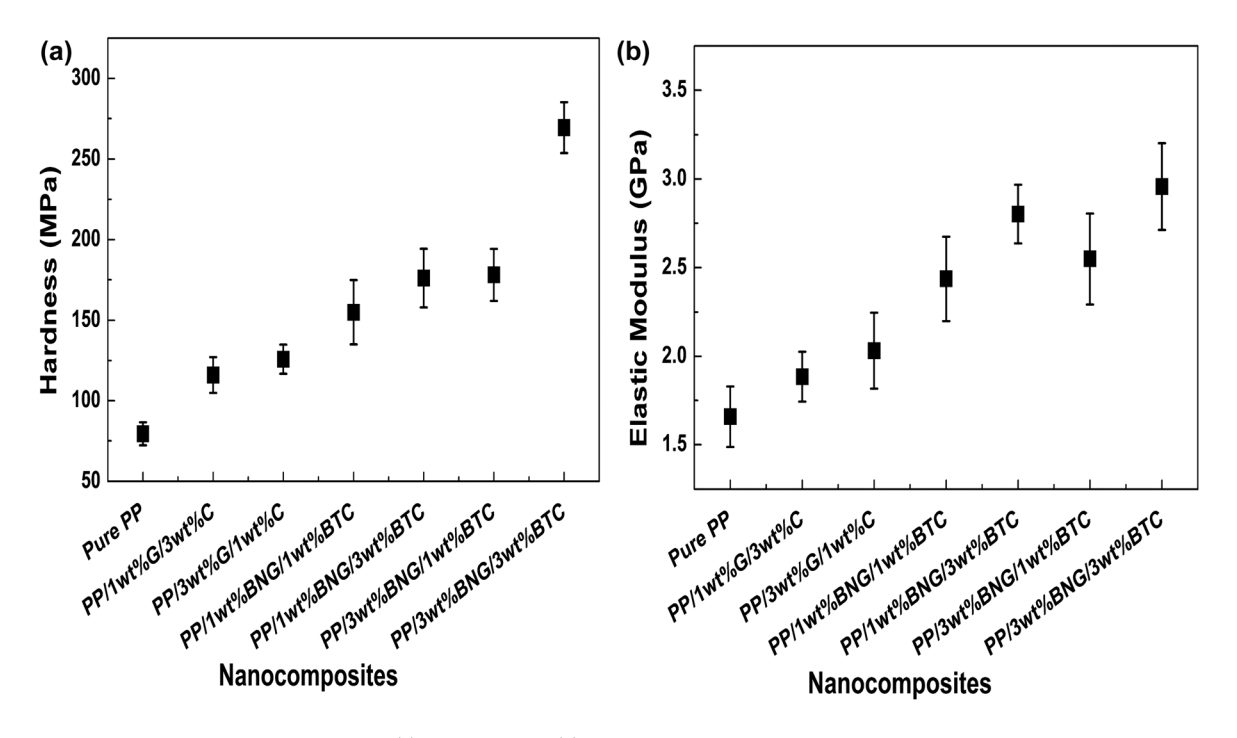


Figure 6: Nanomechanical properties: (a) Hardness and (b) elastic modulus of the nanocomposites.

were achieved with PP/BNG/BTC based nanocomposites compared to their counterparts. This is due to the presence of the BN and BT nanoparticles, which gave the PP/BNG/BTC dense microstructures (SEM micrograph in Figure 3) and more stiffness snice BT could fill microvoids in the nanocomposites owning to its 0D and spherical structure (TEM micrograph in Figure 2). This was more pronounced as the BNG and BTC net concentration increase from 2 wt% to 6 wt% as depicted in Figure 6. This could be as a result of more interaction of the indenter's tip with the nanoparticles than the matrix as the net wt% of the nanoparticles increases [51]. This is an indication that more interlocking and network structural hardening of the PP chains was achieved due to the combination of various nanoparticles with different structural dimensions.

3.6 Creep resistance and force displacement

It is believed that when load was applied, propagating microcracks and PP chains encounter the nanoparticles (obstacles) in the PP matrix with retardation in their mobilities to find new directions. This phenomenon enhanced the mechanical properties of the developed nanocomposites. This was more pronounced for nanocomposites containing BNG and BTC since they comprise different nanoparticles sizes, structures, and orientation in

the matrix. Based on that, the PP/BNG/BTC group showed better creep resistance compared to the pure PP and PP/G/ C group (see Figure 7(a)). The PP/3 wt%BNG/3 wt%BTC nanocomposite also has lower creep (about 4.3%) compared to that of the pure PP (about 10.5%). The creep variation of other nanocomposites in respect to nanoparticles combination and concentration is included in Figure 7(a). The optimal reduction in creep of the PP/BNG/ BTC nanocomposites can be attributed to effective interlocking of the PP chains, uniform dispersion and adhesion of the nanoparticles with the matrix, which are required for improvement of creep resistance [52]. The loadingunloading curves of the nanocomposites obtained from the nanoindentation are represented in Figure 7(b). Due to the earlier stated network structural hardening of the PP matrix, all the nanocomposites showed reduction in maximum and final penetration depth. The reduction in the penetration depth is more pronounced for PP/BNG/BTC nanocomposites group, which agrees with their higher H and EM. This simply means high resistance to change in dimension on the application and removal of load, indicating large stiffness and resistance to elastic deformation due to the network hardening of the PP matrix by the nanoparticles' combination. Rigidity and plastic deformation resistance of the nanocomposites were evaluated in terms of EM to H ratio as presented in Figure 8. The pure PP has higher EM/H ratio (see Figure 8(a)) compared to all the developed nanocomposites. This shows that the rigidity of

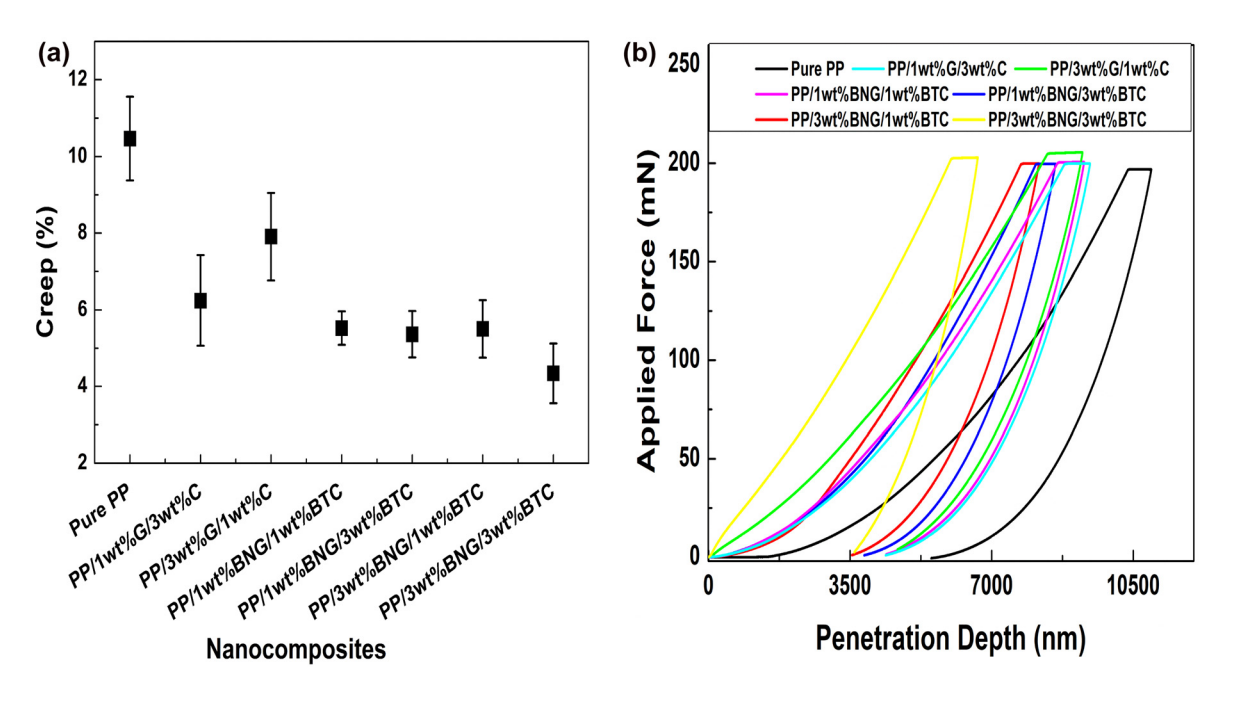


Figure 7: Nanomechanical properties: (a) Creep and (b) force-displacement of the nanocomposites.

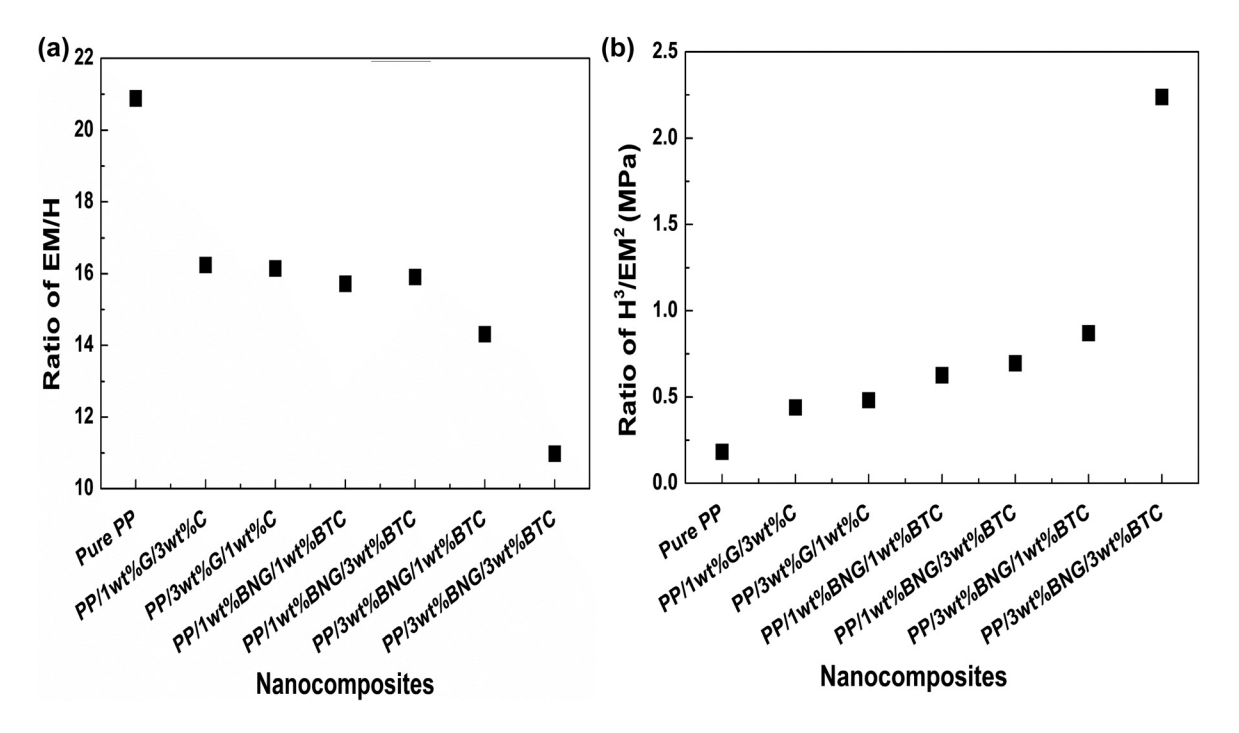


Figure 8: Ratio of (a) EM/H and (b) H³/EM² of the nanocomposites.

the PP matrix increased with addition of the nanoparticles. The nanoparticles were able to restrain the movement of the PP chains on the application of load. The increase in rigidity was more pronounced for the nanocomposites containing BNG/BTC than that of PP/G/C nanocomposites at all concentrations. This can be credited to the denser

microstructure of the PP/BNG/BTC nanocomposites as revealed by the SEM micrographs due to the presence of the BN and BT nanoparticles. The high values of H³/EM² ratio as shown in Figure 8(b) suggests larger resistance to plastic deformation and elasticity of the nanocomposites compared to the pure PP [19, 21] due to the network

hardening of the PP matrix with hybrid carbon and ceramic nanoparticles having 0D, 1D and 2D structures.

3.7 Heat deflection and Vicat softening temperature

The heat deflection temperature (HDT) and Vicat softening temperature (VST) of the nanocomposites are presented in Figure 9. The figure shows that the resistance to deformation of PP matrix under simultaneous application of heat and load increased by the addition of the nanoparticles into the matrix. Figure 9(a) shows that the pure PP deflected by 0.25 mm at 81.7 °C, while incorporation of 3 wt%BNG/3 wt%BTC to its matrix amounted to 100.7 °C before the 0.25 mm deflection. It implies that the nanocomposite has about 19 °C higher deflection temperature compared to the pure PP. The observed increase in the HDT suggests that the PP matrix was stiffening and its chains were controlled against mobility with increase in resistance to deformation [53]. In general, the high aspect ratio of GNs and CNTs and their interconnections in the PP matrix enabled fast dissipation of heat and resistance to bending. While the presence of BN and BT aided in the dispersion, bonding with the matrix, interlocking and

stiffening of the PP matrix. Hence, larger HDT was measured for all the PP/BNG/BTC group compared to the PP/G/C group at similar content. On the other hand, it was also noted that VST of the nanocomposites also increased with addition of the nanoparticles into the PP matrix as shown in Figure 9(b). Just like the HDT, the VST is also higher for PP/BNG/BTC nanocomposites compared to their counterparts. However, the VST values for PP/G/C nanocomposites were still larger compared to the pure PP. Since formation of 3D network structures in the polymer matrix by the interpenetration of the GNs and CNTs can enhance heat conduction and dissipation [54], it implies there was reduction in the accumulation of heat that would have resulted to early softening of the nanocomposites. Hence, it took higher temperature to soften the nanocomposites before penetration of the flat-ended needle by 1.0 mm when compared with the pure PP. In addition, the adjacent nanoparticles to the flat-ended needle restricted the flow of the adjacent PP chains, which gave rise to higher resistance to the pin's penetration. The high VST values of the PP/ BNG/BTC nanocomposites confirms that large network structural interlocking of the PP matrix was achieved in the matrix. Therefore, the VST increased from 148.7 °C for the pure PP to optimal of about 159.8 °C for PP/3 wt%BNG/3 wt %BTC nanocomposite, resulting to about 11.1 °C increase.

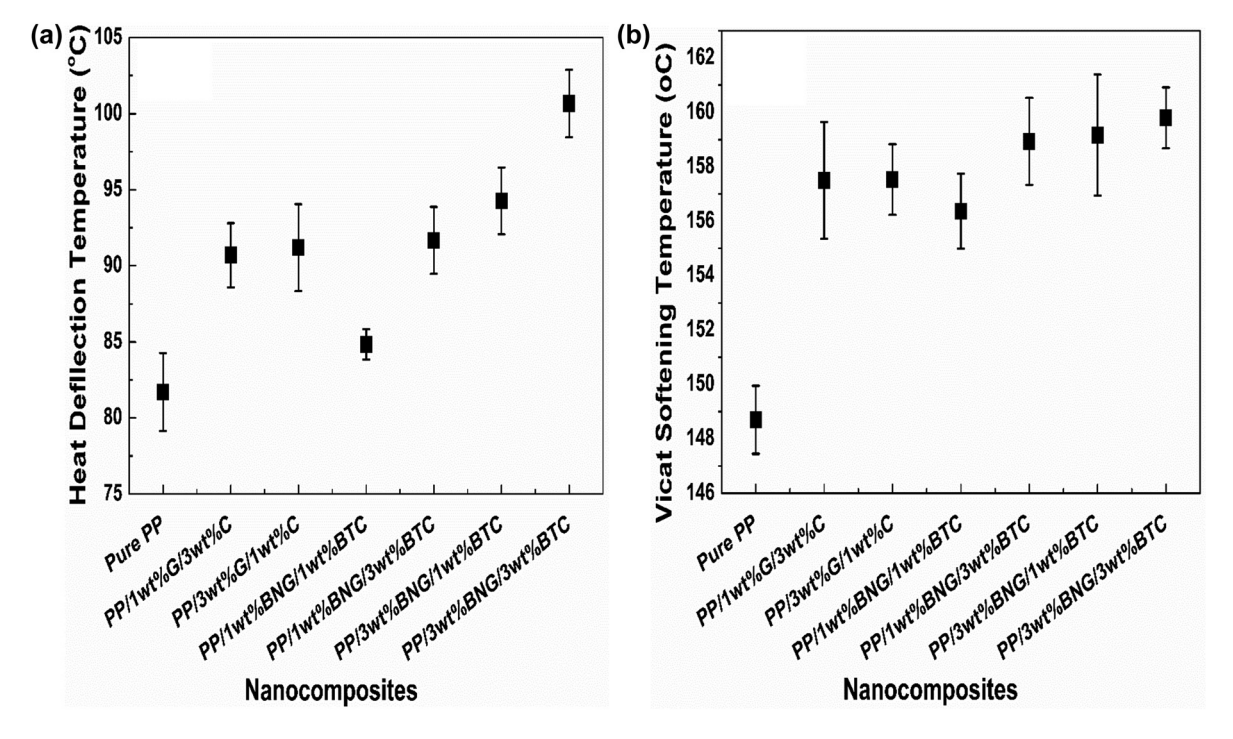


Figure 9: Thermomechanical properties: (a) Heat deflection and (b) Vicat softening temperature of the nanocomposites.

4 Conclusions

The nanocomposites were fabricated via PPMA/nanoparticles masterbatch preparation and subsequent melt compounding with pure PP. The nanocomposites showed significant improvement in the measured mechanical and thermomechanical properties. The enhanced properties were credited to the network structural hardening of the PP matrix, which restricted its chains' mobility on the application of load. The enhanced mechanical and thermomechanical properties were correlated to the mechanical interlocking of the PP chains, efficient load transfer from the matrix to nanoparticles and the network configurations of the microstructures of the nanocomposites as revealed by their SEM micrographs. The presence of the BN and BT nanoparticles resulted to denser morphologies of the nanocomposites and efficient load transfer. Therefore, the PP/BNG/BTC nanocomposites group showed higher hardness, elastic modulus, tensile strength/modulus, heat deflection and Vicat softening temperature. The developed nanocomposites can find advanced mechanical and structural applications owing to their enhanced mechanical properties.

Acknowledgements: We appreciate the Faculty of Engineering and the Built Environment and the Centre for Energy and Electric Power, Tshwane University of Technology, South Africa for their support.

Author contribution: All the authors have accepted responsibility for the entire content of this submitted manuscript and approved submission.

Research funding: None declared.

Conflict of interest statement: The authors declare that they have no conflicts of interest regarding this article.

References

- 1. Rajeshwari P., Dey T. Novel hdpe nanocomposites containing aluminum nitride (nano) particles: micro-structural and nanomechanical properties correlation. Mater. Chem. Phys. 2017, 190, 175-186.
- 2. Puértolas J., Castro M., Morris J., Ríos R., Ansón-Casaos A. Tribological and mechanical properties of graphene nanoplatelet/peek composites. Carbon 2019, 141, 107-122.
- 3. Ike-Eze I. E., Uyor U., Aigbodion V., Omah A., Ude S., Daniel-Nkpume C. Tensile and compressive strength of palm kernel shell particle reinforced polyester composites. Mater. Res. Express 2019, 6, 1-7.
- 4. Mora A., Verma P., Kumar S. Electrical conductivity of cnt/ polymer composites: 3d printing, measurements and modeling. Compos. B Eng. 2020, 183, 107600.

- 5. Salehi S., Maghmoomi F., Sahebian S., Zebarjad S., Lazzeri A. A study on the effect of carbon nanotube surface modification on mechanical and thermal properties of cnt/hdpe nanocomposite. J. Thermoplast. Compos. Mater. 2021, 34, 203-220.
- 6. Kuila T., Bose S., Mishra A. K., Khanra P., Kim N. H., Lee J. H. Chemical functionalization of graphene and its applications. Prog. Mater. Sci. 2012, 57, 1061-1105.
- 7. Huang X., Jiang P., Tanaka T. A review of dielectric polymer composites with high thermal conductivity. IEEE Electr. Insul. Mag. 2011, 27, 8-16.
- 8. Chrissafis K., Bikiaris D. Can nanoparticles really enhance thermal stability of polymers? Part i: an overview on thermal decomposition of addition polymers. Thermochim. Acta 2011, 523, 1-24.
- 9. Garzón C., Palza H. Electrical behavior of polypropylene composites melt mixed with carbon-based particles: effect of the kind of particle and annealing process. Compos. Sci. Technol. 2014, 99, 117-123.
- 10. Uyor U., Popoola O., Aigbodion V. Advanced rheological and mechanical properties of three-phase polymer nanocomposites through strong interfacial interaction of graphene and titania. Int. J. Adv. Manuf. Technol. 2019, 104, 1311-1319.
- 11. Papanicolaou G., Charitidis C., Portan D., Perivoliotis D., Koklioti M. Investigation of nanomechanical properties of multilayered hybrid nanocomposites. Meccanica 2014, 49, 2645-2655.
- 12. Mansor M., Fadzullah S., Masripan N., Omar G., Akop M. Comparison between functionalized graphene and carbon nanotubes: effect of morphology and surface group on mechanical, electrical, and thermal properties of nanocomposites. In: Functionalized Graphene Nanocomposites and their Derivatives. Elsevier; 2019. pp. 177-204.
- 13. Azo M. Boron Nitride (BN) Properties and Information on Boron Nitride; 2001. https://www.azom.com/article.aspx?ArticleID=78 [accessed April 10, 2020].
- 14. Azo M. Barium Titanate (BaTiO₃) Properties and Applications; 2004. https://www.azom.com/article.aspx?ArticleID=2280 [accessed February 14, 2022].
- 15. Uyor U., Popoola A., Popoola O., Aigbodion V. Nanomechanical evaluation of poly (vinylidene fluoride) nanocomposites reinforced with hybrid graphene nanoplatelets and titanium dioxide. Polym. Bull. 2021, 79, 1-17.
- 16. Sreeram A., Patel N. G., Venkatanarayanan R. I., McLaughlin J. B., DeLuca S. J., Yuya P. A., Krishnan S. Nanomechanical properties of poly (para-phenylene vinylene) determined using quasi-static and dynamic nanoindentation. Polym. Test. 2014, 37, 86-93.
- 17. Dada M., Popoola P., Mathe N., Adeosun S., Pityana S. Investigating the elastic modulus and hardness properties of a high entropy alloy coating using nanoindentation. Int. J. Lightweight Mater. Manuf. 2021, 4, 339-345.
- 18. Chafidz A., Rengga W. D. P., Khan R., Kaavessina M., Almutlaq A. M., Almasry W. A., Ajbar A. Polypropylene/multiwall carbon nanotubes nanocomposites: nanoindentation, dynamic mechanical, and electrical properties. J. Appl. Polym. Sci. 2017, 134, 45293.
- 19. Tserpes K., Chanteli A., Pantelakis S., Koumoulos E., Charitidis C. Mechanical and nanomechanical properties of mwcnt/pp nanocomposite. Frat. Ed. Integrità Strutt. 2018, 12, 73-83.
- 20. Yetgin S. H. Effect of multi walled carbon nanotube on mechanical, thermal and rheological properties of polypropylene. J. Mater. Res. Technol. 2019, 8, 4725-4735.

- 21. Koumoulos E. P., Jagdale P., Kartsonakis I. A., Giorcelli M., Tagliaferro A., Charitidis C. A. Carbon nanotube/polymer nanocomposites: a study on mechanical integrity through nanoindentation. Polym. Compos. 2015, 36, 1432-1446.
- 22. Wan Q., Liu M., Tian J., Deng F., Dai Y., Wang K., Li Z., Zhang Q., Zhang X., Wei Y. Toward the development of versatile functionalized carbon nanotubes. RSC Adv. 2015, 5, 38316-38323.
- 23. Zhou Z., Wang S., Lu L., Zhang Y., Zhang Y. Functionalization of multi-wall carbon nanotubes with silane and its reinforcement on polypropylene composites. Compos. Sci. Technol. 2008, 68, 1727-1733.
- 24. Liu F., Wu L., Song Y., Xia W., Guo K. Effect of molecular chain length on the properties of amine-functionalized graphene oxide nanosheets/epoxy resins nanocomposites. RSC Adv. 2015, 5, 45987-45995.
- 25. Li Y., Fan M., Wu K., Yu F., Chai S., Chen F., Fu Q. Polydopamine coating layer on graphene for suppressing loss tangent and enhancing dielectric constant of poly(vinylidene fluoride)/ graphene composites. Compos. Appl. Sci. Manuf. 2015, 73, 85-92.
- 26. Ahmed K., Kanwal F., Ramay S. M., Atiq S., Rehman R., Ali S. M., Alzayed N. S. Synthesis and characterization of batio3/ polypyrrole composites with exceptional dielectric behaviour. Polymers 2018, 10, 1273.
- 27. Wu L., Wu K., Lei C., Liu D., Du R., Chen F., Fu Q. Surface modifications of boron nitride nanosheets for poly (vinylidene fluoride) based film capacitors: advantages of edgehydroxylation. J. Mater. Chem. 2019, 7, 7664-7674.
- 28. Yang N., Yang T., Wang W., Chen H., Li W. Polydopamine modified polyaniline-graphene oxide composite for enhancement of corrosion resistance. J. Hazard Mater. 2019, 377, 142-151.
- 29. Li H., Xu C., Chen Z., Jiang M., Xiong C. Graphene/poly(vinylidene fluoride) dielectric composites with polydopamine as interface layers. Sci. Eng. Compos. Mater. 2017, 24, 327-333.
- 30. Geick R., Perry C., Rupprecht G. Normal modes in hexagonal boron nitride. Phys. Rev. 1966, 146, 543-547.
- 31. Gonzalez Ortiz D., Pochat-Bohatier C., Cambedouzou J., Bechelany M., Miele P. Exfoliation of hexagonal boron nitride (h-bn) in liquid phase by ion intercalation. Nanomaterials 2018, 8, 1-12.
- 32. Sudeep P. M., Vinod S., Ozden S., Sruthi R., Kukovecz A., Konya Z., Vajtai R., Anantharaman M., Ajayan P. M., Narayanan T. N. Functionalized boron nitride porous solids. RSC Adv. 2015, 5, 93964-93968.
- 33. Cao X. T., Showkat A. M., Lee W.-K., Lim K. T. Luminescence of terbium (iii) complexes incorporated in carboxylic acid functionalized polystyrene/batio3 nanocomposites. Mol. Cryst. Lig. Cryst. 2015, 622, 36-43.
- 34. Phan T. T. M., Chu N. C., Xuan H. N., Pham D. T., Martin I., Carrière P. Enhancement of polarization property of silanemodified batio3 nanoparticles and its effect in increasing dielectric property of epoxy/BaTiO₃ nanocomposites. J. Sci: Adv. Mater. Devices 2016, 1, 90-97.
- 35. Chang S.-J., Liao W.-S., Ciou C.-J., Lee J.-T., Li C.-C. An efficient approach to derive hydroxyl groups on the surface of barium titanate nanoparticles to improve its chemical modification ability. J. Colloid Interface Sci. 2009, 329, 300-305.

- 36. Jun Y.-S., Um J. G., Jiang G., Lui G., Yu A. Ultra-large sized graphene nano-platelets (gnps) incorporated polypropylene (pp)/gnps composites engineered by melt compounding and its thermal, mechanical, and electrical properties. Compos. B Eng. 2018, 133, 218-225.
- 37. Li C.-Q., Zha J.-W., Long H.-Q., Wang S.-J., Zhang D.-L., Dang Z.-M. Mechanical and dielectric properties of graphene incorporated polypropylene nanocomposites using polypropylene-graftmaleic anhydride as a compatibilizer. Compos. Sci. Technol. 2017, 153, 111-118.
- 38. Liem H., Choy H. Superior thermal conductivity of polymer nanocomposites by using graphene and boron nitride as fillers. Solid State Commun. 2013, 163, 41-45.
- 39. Xiao Y.-j., Wang W.-v., Chen X.-j., Lin T., Zhang Y.-t., Yang J.-h., Wang Y., Zhou Z.-w. Hybrid network structure and thermal conductive properties in poly(vinylidene fluoride) composites based on carbon nanotubes and graphene nanoplatelets. Compos. Appl. Sci. Manuf. 2016, 90, 614-625.
- 40. Zhang G., Wang F., Dai J., Huang Z. Effect of functionalization of graphene nanoplatelets on the mechanical and thermal properties of silicone rubber composites. Materials 2016, 9, 1-13.
- 41. Miltner H. E., Grossiord N., Lu K., Loos J., Koning C. E., Van Mele B. Isotactic polypropylene/carbon nanotube composites prepared by latex technology. Thermal analysis of carbon nanotubeinduced nucleation. Macromolecules 2008, 41, 5753-5762.
- 42. Kazemi Y., Kakroodi A. R., Wang S., Ameli A., Filleter T., Pötschke P., Park C. B. Conductive network formation and destruction in polypropylene/carbon nanotube composites via crystal control using supercritical carbon dioxide. Polymer 2017, 129, 179-188.
- 43. Roh J. U., Ma S. W., Lee W. I., Hahn H. T., Lee D. W. Electrical and mechanical properties of graphite/maleic anhydride grafted polypropylene nanocomposites. Compos. B Eng. 2013, 45, 1548-1553.
- 44. Nurul M., Mariatti M. Effect of thermal conductive fillers on the properties of polypropylene composites. J. Thermoplast. Compos. Mater. 2013, 26, 627-639.
- 45. Li Z., Chen M., Ma W. Polypropylene/hydroxyl-multiwall carbon nanotubes composites: crystallization behavior, mechanical properties, and foaming performance. J. Mater. Sci. 2016, 51, 4566-4579.
- 46. Li J. Multiwalled carbon nanotubes reinforced polypropylene composite material. J. Nanomater. 2017, 2017, 1-5.
- 47. Chen B., Li X., Jia Y., Xu L., Liang H., Li X., Yang J., Li C., Yan F. Fabrication of ternary hybrid of carbon nanotubes/graphene oxide/mos2 and its enhancement on the tribological properties of epoxy composite coatings. Compos. Appl. Sci. Manuf. 2018, 115, 157-165.
- 48. Yang J., Zhang Z., Friedrich K., Schlarb A. K. Creep resistant polymer nanocomposites reinforced with multiwalled carbon nanotubes. Macromol. Rapid Commun. 2007, 28, 955-961.
- 49. Bhattacharyya A., Chen S., Zhu M. Graphene reinforced ultra high molecular weight polyethylene with improved tensile strength and creep resistance properties. Express Polym. Lett. 2014, 8, 74-84.
- 50. Díez-Pascual A. M., Gómez-Fatou M. A., Ania F., Flores A. Nanoindentation in polymer nanocomposites. Prog. Mater. Sci. 2015, 67, 1-94.

- 51. Shokrieh M., Hosseinkhani M., Naimi-Jamal M., Tourani H. Nanoindentation and nanoscratch investigations on graphene-based nanocomposites. Polym. Test. 2013, 32, 45-51.
- 52. Hassanzadeh-Aghdam M. K., Mahmoodi M. J., Ansari R. Creep performance of cnt polymer nanocomposites-an emphasis on viscoelastic interphase and cnt agglomeration. Compos. B Eng. 2019, 168, 274-281.
- 53. Ghoshal S., Wang P.-H., Gulgunje P., Verghese N., Kumar S. High impact strength polypropylene containing carbon nanotubes. Polymer 2016, 100, 259-274.
- 54. Yu J., Choi H. K., Kim H. S., Kim S. Y. Synergistic effect of hybrid graphene nanoplatelet and multi-walled carbon nanotube fillers on the thermal conductivity of polymer composites and theoretical modeling of the synergistic effect. Compos. Appl. Sci. Manuf. 2016, 88, 79-85.